

This work was written as part of one of the author's official duties as an Employee of the United States Government and is therefore a work of the United States Government. In accordance with 17 U.S.C. 105, no copyright protection is available for such works under U.S. Law.

Public Domain Mark 1.0

<https://creativecommons.org/publicdomain/mark/1.0/>

Access to this work was provided by the University of Maryland, Baltimore County (UMBC) ScholarWorks@UMBC digital repository on the Maryland Shared Open Access (MD-SOAR) platform.

**Please provide feedback**

Please support the ScholarWorks@UMBC repository by emailing [scholarworks-group@umbc.edu](mailto:scholarworks-group@umbc.edu) and telling us what having access to this work means to you and why it's important to you. Thank you.

# PROCEEDINGS OF SPIE

[SPIDigitalLibrary.org/conference-proceedings-of-spie](https://spiedigitallibrary.org/conference-proceedings-of-spie)

## Design, analysis, and testing of x-ray mirror modules

Peter Solly, Michael Biskach, Kai-Wing Chan, James Mazzarella, Ryan McClelland, et al.

Peter M. Solly, Michael Biskach, Kai-Wing Chan, James Mazzarella, Ryan E. McClelland, Raul Riveros, Timo T. Saha, William W. Zhang, "Design, analysis, and testing of x-ray mirror modules," Proc. SPIE 12181, Space Telescopes and Instrumentation 2022: Ultraviolet to Gamma Ray, 121814O (31 August 2022); doi: 10.1117/12.2629536

**SPIE.**

Event: SPIE Astronomical Telescopes + Instrumentation, 2022, Montréal, Québec, Canada

# Design, Analysis, and Testing of X-ray Mirror Modules

Peter M. Solly<sup>\*a,c</sup>, Michael Biskach<sup>c</sup>, Kai-Wing Chan<sup>b,c</sup>, James Mazzarella<sup>a,c</sup>, Ryan McClelland<sup>c</sup>, Raul E. Riveros<sup>b,c</sup>, Timo T. Saha<sup>c</sup>, William W. Zhang<sup>c</sup>

<sup>a</sup>KBR Space Engineering Division, 7701 Greenbelt Road, Suite 400, Greenbelt, Maryland 20770, USA

<sup>b</sup>Center for Research and Exploration in Space Science and Technology & University of Maryland, Baltimore County, Baltimore, MD 21250, USA

<sup>c</sup>NASA Goddard Space Flight Center (GSFC), Greenbelt, MD USA 20771, USA

## ABSTRACT

The construction of X-ray telescopes that exhibit both high resolution and a low mass to effective area ratio poses many unique challenges. As the development of lightweight silicon X-ray mirrors approaches sub-arc-second resolution, previously inconsequential effects and complications must be addressed. This paper will address the structural analysis methods and experimental data that has been collected in attempts to address and resolve these issues for silicon mirror modules. Various parameters are run through trade space using Finite Element (FE) models and ray trace algorithms in attempts to contribute to the understanding of challenging and extremely sensitive conditions. Results and experimental data are then used to guide the on-going development of optics modules meeting the requirements of ambitious future X-ray missions. In this paper we discuss how the stringent distortion requirements of a high-resolution telescope are combined with launch vibration strength requirements to design optimized mirror modules.

**Keywords:** silicon mirrors, module, mirror assembly, X-ray optics, structural analysis, optimization, finite element model

\*Peter M Solly, peter.m.solly@nasa.gov

## 1. INTRODUCTION

Polished silicon X-ray optics [1] are the most promising technology for mirror assemblies, the most critical component of potential high-resolution X-ray telescopes. This segmented technology is applicable to missions of all sizes, from sounding rocket missions such as OGRE [2] and MIDEX missions such as STAR-X [3] to flagship missions such as Lynx [4]. A simplified assembly process is shown in Figure 1-1.

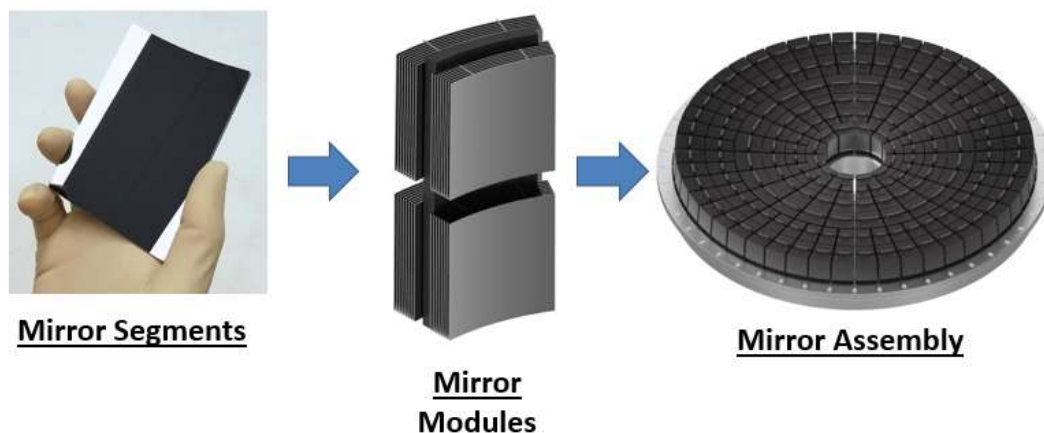


Figure 1-1 Polished Silicon Mirrors from Segment to Mirror Assembly

Individual mirror segments with approximate dimensions of 100mm length and height and 0.5mm thickness, are manufactured using polishing techniques [5] and Ion Beam Figuring (IBF) to surface precisions equaling or exceeding the Chandra X-ray Observatory [6]. These mirror segments are then aligned and bonded into Mirror Modules [7], stacked on top of each other using four ideally located bond points that are integrated into the back surface of the mirror and control the precision alignment. The mirror module can be designed as a robust structure, able to be subjected to structural verification tests to verify the strength of the mirrors and bonds, as well as the stability of the X-ray performance and characterization. These modules will then be integrated into a large Mirror Assembly structure, co-aligned to high precision. Of these steps, the bonding of mirror segments into modules and subsequent structural verification, combined with maintaining high quality x-ray performance, remain some of the most challenging issues in the development of this technology. The stacking nature of the mirror modules necessitates large bonds at the innermost mirrors to achieve survivability but increasing bond size can cause significant distortion to the mirror via epoxy shrinkage effects. This paper will detail the structural verification tests that have been performed to date, as well as analytical methods that have been developed to characterize the impacts to optical performance of the mirror bonding process.

## 2. STRUCTURAL VERIFICATION

Previous testing for silicon mirrors included material characterization, as well as random, sine, and shock vibration of a single mirror with a mass simulator representing 24 shells [8]. Those tests were successful, focusing on the robustness of the mirrors and epoxy bonds to withstand launch loads, but did not include X-ray performance verification. The tests presented here take a different approach, focusing on showing consistent X-ray performance after exposure to launch vibration and thermal environments, at the expense of the strength needed for large stacks. This is achieved by testing smaller stacks that are bonded using smaller epoxy bonds to reduce epoxy induced distortion.

### 2.1 Vibration Test

Vibration tests were conducted on the module ABX2103. This module consisted of 5 pairs of mirrors bonded to each other and to a silicon cradle using 1.5mm diameter posts. Three bonded kinematic balls on the base of the cradle are clamped using capture plates to the vibration table adapter plate. Teardrop accelerometers are attached to the outermost mirrors to monitor mirror responses. The test article on shaker table is shown in Figure 2-1.

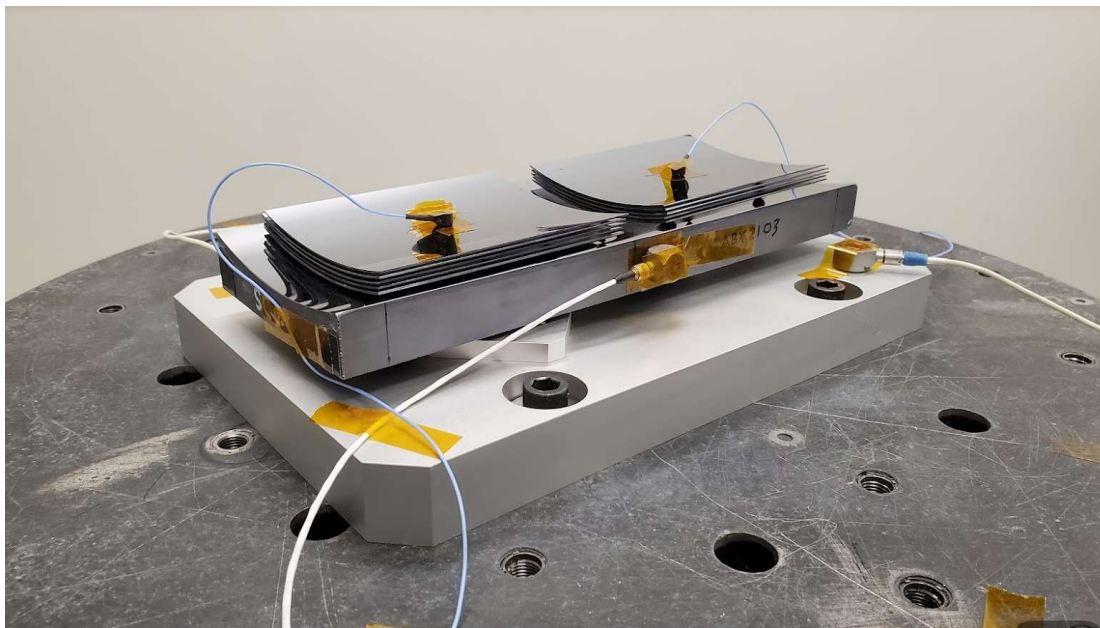


Figure 2-1 ABX2103 Vibration Test Setup

The module was subjected to both random vibration and sine burst vibrations. Pre and post low level sine sweeps were conducted after each test to confirm structural integrity. The sine burst levels applied were 12.3 G's in the Axial (optical axis) direction, and 3.4 G's in the radial/tangential directions, derived from IXO CLA loads [9] with a 2.0 uncertainty factor applied. The random vibration input applied was GEVS minimum workmanship [10], with notches at high frequencies to account for the hard mounted structure, as a flight like module would be mounted with flexures. The input Power Spectral Density (PSD) function can be seen in Figure 2-2.

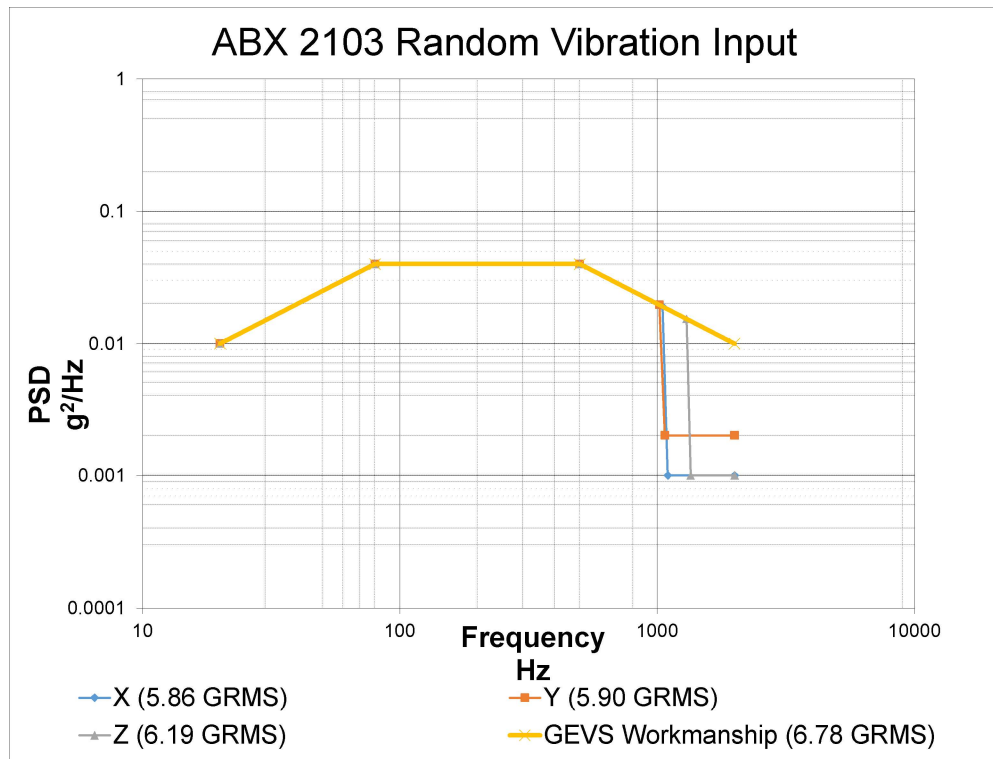


Figure 2-2 ABX2103 Random Vibration Input Spectrums

A summary of the measured responses can be seen in Table 2-1, compared to the predicted responses from the FEM shown in Figure 2-3. Note mirror responses are only in the radial direction, as the teardrop accelerometers used are single axis.

Table 2-1 ABX2103 Random Vibration GRMS Output Summary

Range	Input	Baseplate	Cradle			Primary	Secondary
	X	X	X	Y	Z	X	X
Prediction	5.87	6.02	6.77	0.06	0.50	16.88	8.42
Actual	5.86	5.74	6.87	0.61	2.86	18.12	9.74

Range	Input	Baseplate	Cradle			Primary	Secondary
	Y	Y	X	Y	Z	X	X
Prediction	6.04	6.11	4.22	6.76	0.38	0.08	0.02
Actual	5.85	5.86	8.73	7.67	3.00	6.05	6.27

Range	Input	Baseplate	Cradle			Primary	Secondary
	Z	Z	X	Y	Z	X	X
Prediction	6.17	6.20	1.47	0.05	6.73	6.20	3.16
Actual	6.17	6.21	3.19	0.91	9.45	18.28	7.43

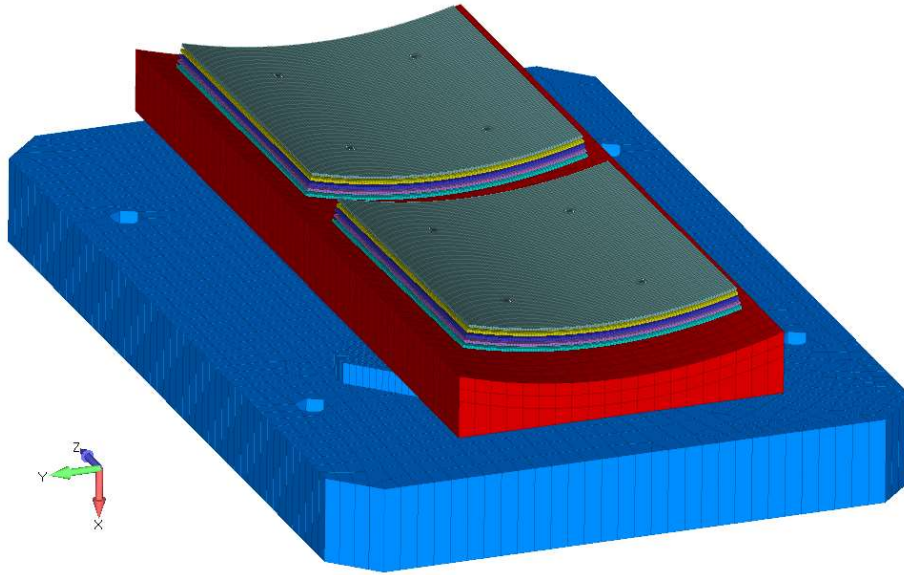


Figure 2-3 ABX2103 Vibration FEM

Most of the mirror response occurs at high frequencies above 1000 Hz, despite the notched inputs. This high response is well matched to the model predictions, a detailed plot of the measured PSD response from the radial input along with model prediction for the primary mirror is shown in Figure 2-4.

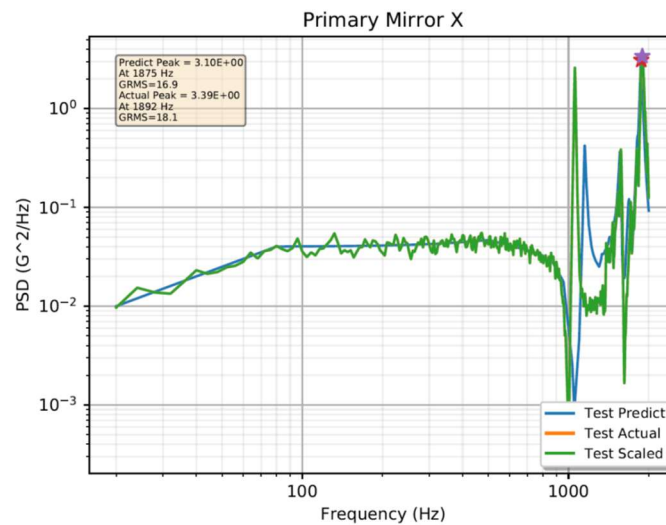
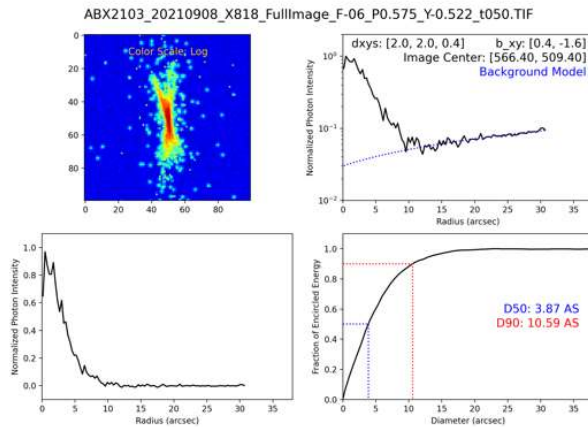


Figure 2-4 Mirror Radial Vibration PSD Response

All sine sweeps indicated structural integrity had been maintained. To confirm that all bonds remained fully intact and that no alignment errors had been introduced, additional X-ray testing was performed after the vibration testing. This testing confirmed that the module was still aligned and performing well, the HPD had increased from 3.9" to 4.2", but that amount of change is well within variation seen between repeat X-ray tests, and within other measurements taken of this module. Detailed image plots can be seen in Figure 2-5.

## Pre-Vibration Test



## Post-Vibration Test

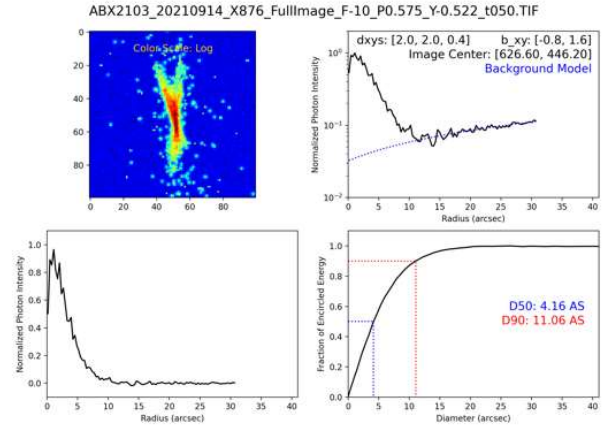


Figure 2-5 ABX2103 Comparison of Pre-Vibration and Post-Vibration X-ray Testing

## 2.2 Thermal Vacuum Test

To confirm that the epoxy bonds can withstand significant temperature variations without permanent effects on optical performance, TVAC testing was performed on another 5 pair module, ABX2102. This module is nearly identical to that used in the vibration test outlined in the previous section. The module in TVAC chamber is shown in Figure 2-6.

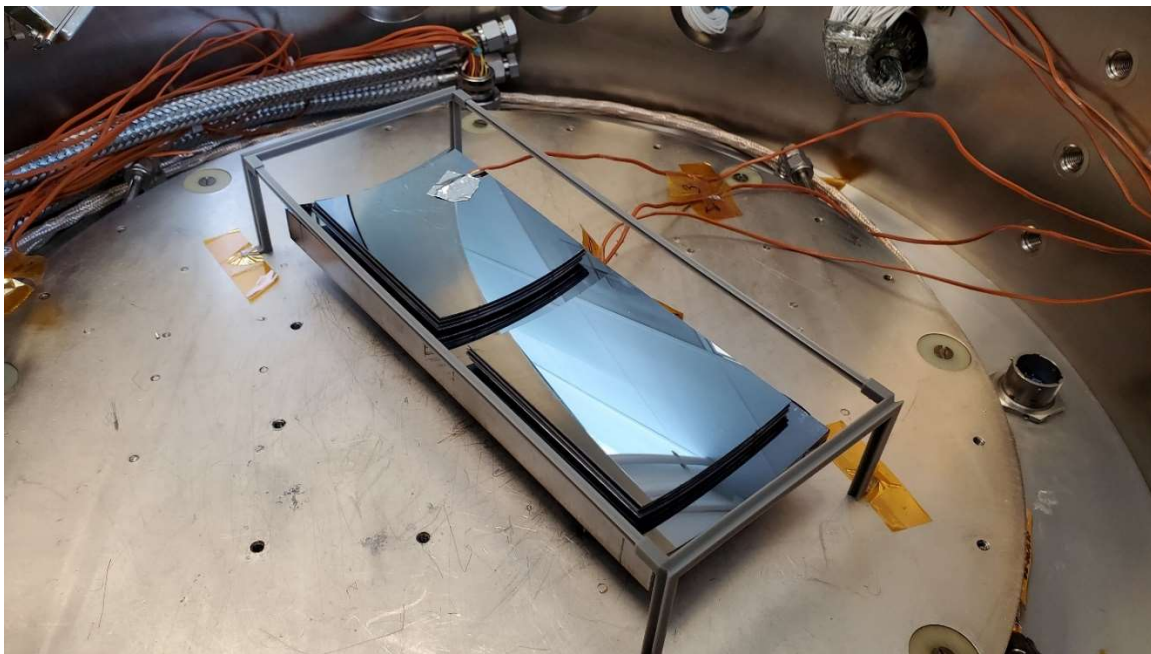


Figure 2-6 ABX2102 In TVAC Chamber

The goal of the test was to cycle the test article five times between the temperatures of 0 °C and 40 °C. Due to limited conductive coupling between the test article and the cold plate used to drive the temperatures, the actual temperature bounds of the test as measured on the cradle were 1.6 °C and 39.6 °C. This temperature range is considered acceptable for most potential missions. The temperature data recorder during testing is shown in Figure 2-7.

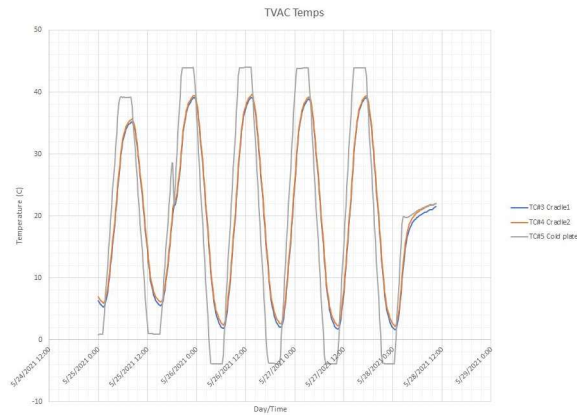


Figure 2-7 ABX2102 TVAC Temperature Data

X-ray testing of the module after TVAC showed no image degradation, the HPD had improved from 3.6" to 3.0", shown in Figure 2-8. These values are in line with the image variation seen during testing due to epoxy desiccation, which ranged in HPD from 2.9" to 4.2".

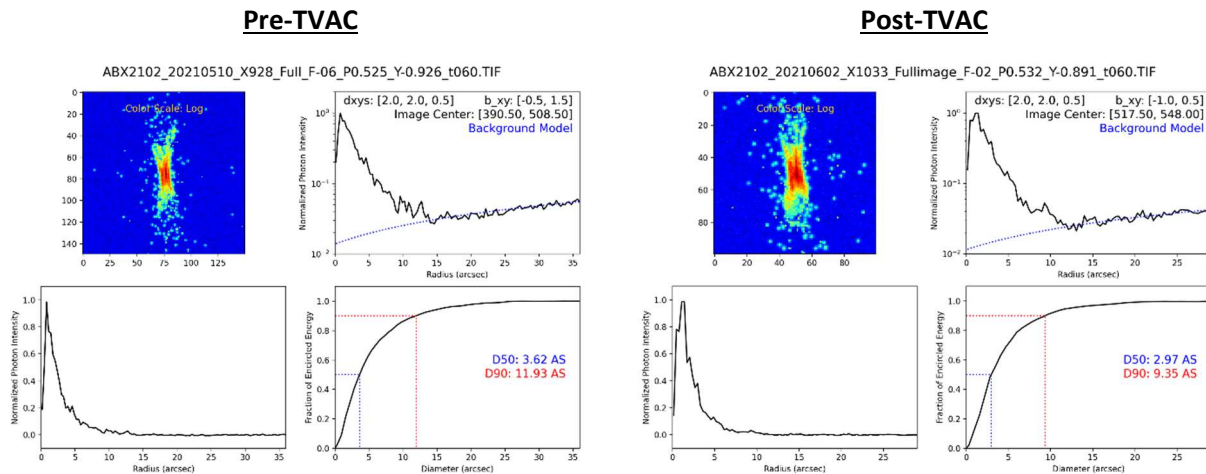


Figure 2-8 ABX2102 Comparison of Pre-TVAC and Post-TVAC X-ray Testing

### 3. BONDING DISTORTION

A significant driver of mirror figure error is distortion caused by the epoxy used to bond the four spacers to the mirror or cradle surface below it. As the epoxy cures it desiccates and shrinks, inducing moments to the surface of the mirror.

#### 3.1 Determining Epoxy Shrinkage

To determine an approximate value of epoxy shrinkage to use for future analysis, a simple experiment was setup using four spacers bonded to the backside of a mirror. These spacers had a diameter of 4.25mm, and a well machined conical tip to provide a known bond gap similar to the ones used in bonding to the mirror surface. The epoxy chosen is Hysol 9313, due to its somewhat unique combination of low outgassing properties, high strength, room temperature cure, and low viscosity, a significant requirement due to the nature of the four point alignment process where the mirror has to repeatably settle into a kinematic position on the four points using applied vibration. A detailed FEM was setup using known material values, with the shrinkage load applied using a temperature difference and adjusted coefficient of thermal expansion applied only to the epoxy elements. The shrinkage values are then adjusted individually at the four epoxy bonds to match the peaks measured on the interferometer. A comparison of a correlated model and

interferometer surface image is shown in Figure 3-1. This distortion was measured after the epoxy had been heat cured at 50 C for 12 hours.

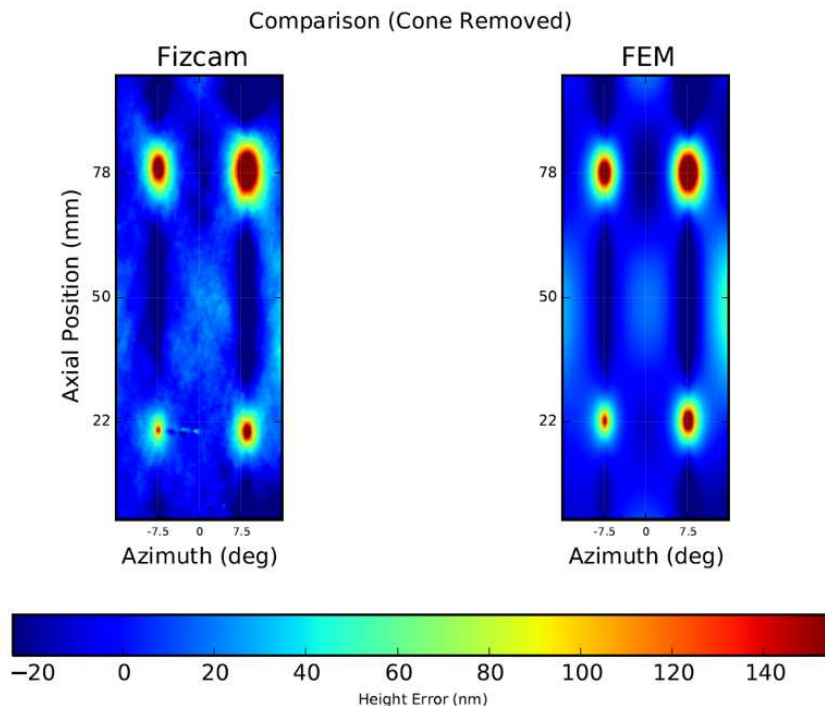


Figure 3-1 Comparison of Epoxy Shrinkage Experimental Measurement With Correlated Model

This experiment was repeated using a different epoxy, Devcon 5 minute diluted with acetone. A summary of the tuned FEM values for the four spacers is shown in Table 3-1.

Table 3-1 Summary of Correlated Epoxy Shrinkage Values

Mirror		330P1080	330P1083
Epoxy		Hysol 9313	Devcon 5min+Acetone
Estimated Cure Strain	BE	0.115%	0.030%
	SE	0.061%	0.174%
	ST	0.104%	0.230%
	BT	0.184%	0.113%
Average:		0.116%	0.137%
Standard Dev:		0.051%	0.085%

The distortion was monitored for four weeks, with repeat measurements showing the distortion receding as the epoxy re-absorbed moisture from being stored in an ambient environment. The sequence of measurements, with bond variation represented as circle size, is plotted in Figure 3-2. Note that the heat cure occurred on day 6 of the curing process.

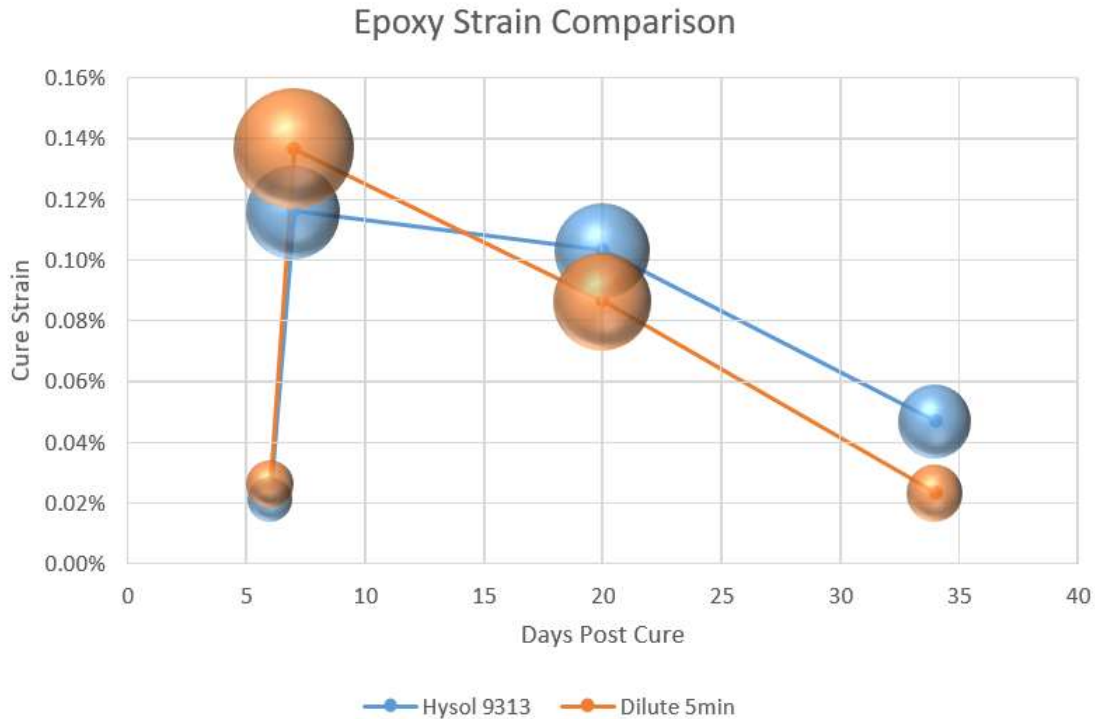


Figure 3-2 Measured Epoxy Shrinkage and Variation Over Time (Heat Cure on Day 6)

Based on this analysis, a shrinkage value of 0.116% can be assumed for Hysol 9313. However the amount of measured variation is significant. When variable values are input into the FEM of a pair of mirrors, the resulting ray trace errors can be significantly higher than applying the mean values at all spacers. For a pair of mirrors 0.6 mm thick, the distortion using the mean strain would be 3.7". For the same model, applying a randomly generated set of strains using the mean and standard deviation from the experimentally correlated values would yield an average mirror distortion of 5.0", with values ranging from 2.5" to 13". The distribution of input strains and output HPD for 1000 randomly generated cases is shown in Figure 3-3.

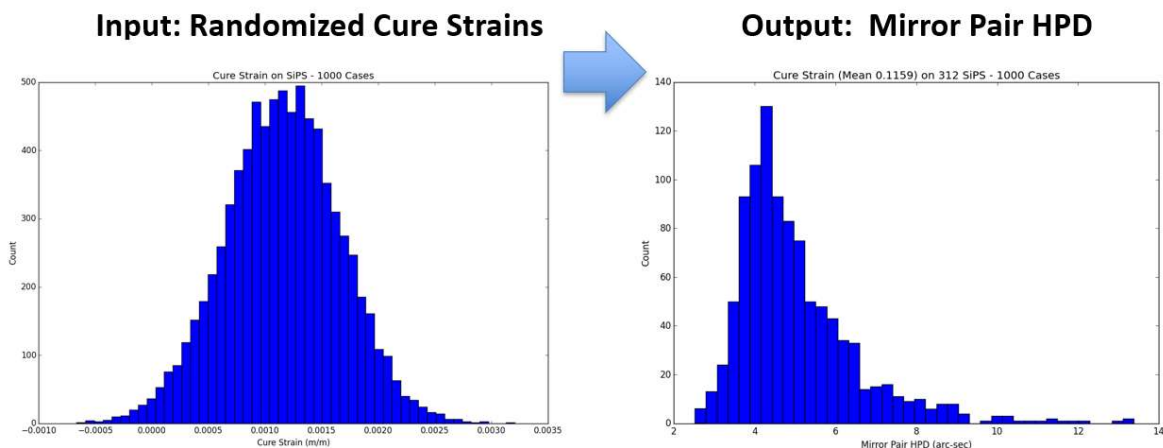


Figure 3-3 Effects of Random Distribution of Epoxy Shrinkage Values on Modeled Mirror Pair Distortion

### 3.2 Sensitivity to Bond Geometry

In addition to variation in epoxy shrinkage, it is also important to consider the impacts of bonding geometry on mirror distortion. The four-point bonds use conically tipped spacers to produce a single discrete point of contact between the spacer and mirror that can be used to deterministically align the mirror using a precision lapping process on the spacer tip. The bond gap is therefore controlled by the angle of the tip of this spacer. This geometry is shown in Figure 3-4, and the predicted bonding distortion for a mirror with these tips is shown in Figure 3-5.

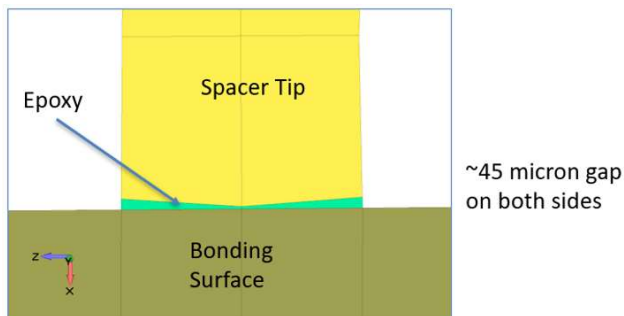


Figure 3-4 Nominal Bonding Geometry

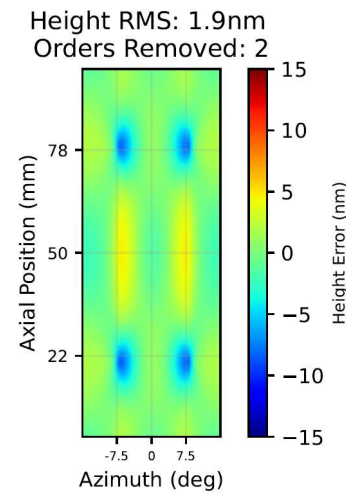


Figure 3-5 Modeled Figure Distortion for Nominal Geometry

The local cone angle of this tip and resulting bond gap can be well controlled. However, the global angle of the spacer tip relative to the bonding surface is much harder to control to a high level of precision. Any error in the global tip angle generates some variation in the bond gap from one side of the spacer to the other. Figure 3-6 shows the geometry if this tip is rotated two degrees, roughly equal to the cone angle of some secondary mirrors that have been produced. This results in significantly more distortion, increasing the surface RMS (sag removed) by an order of magnitude, from 1.9 nm to 18.3 nm, shown in Figure 3-7.

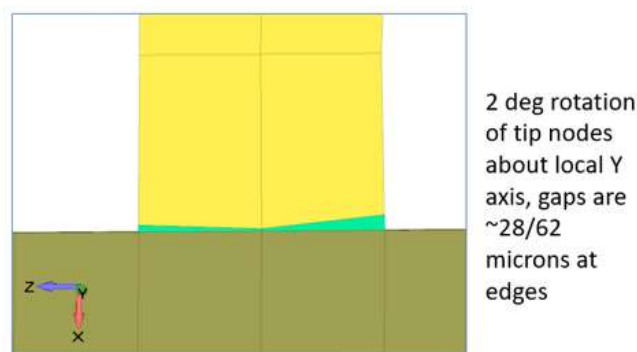


Figure 3-6 Bonding Geometry with 2 degree Angle to Bonding Surface

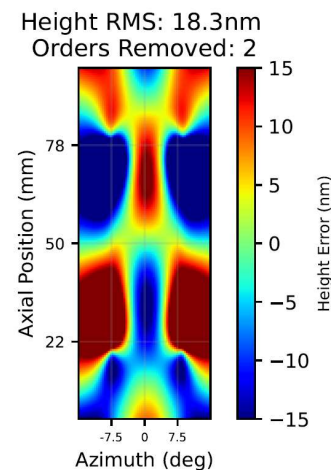


Figure 3-7 Resulting Modeled Distortion with 2 degree Error to Bonding Surface

### 3.3 Stiffening Methods

One potential method of reducing bonding distortion would be to stiffen the mirror itself by adding features to the back surface. Potential geometries are very open ended, as the CNC process used on the back surface to integrate the alignment spacers can be easily modified to add many different features. The limitation of this approach is the spacing required between nested mirrors, which significantly constrains what radial thickness the mirror or mirror features can be. A trade study was performed on a pair of mirrors that were 0.8mm (primary) and 0.9mm (secondary) thick, that had a nominal bond distortion of 2.35" using the modeling techniques previously described. If the mirrors are uniformly increased in thickness to > 2mm, the bonding distortion reduces to 0.46". This however is not ideal, as mirror thickness would then block the reflecting surface of the mirror pair behind it and either significantly reduce effective area or require increased spacing between mirrors and therefore reduce the packing factor of the mirror shells and the resulting aperture space. The most ideal stiffening method for the four-point bonding method would be axial (i.e., along the optical axis direction) ribs located on the same azimuth as the spacers, as they would block mirror aperture that is already effectively blocked by the spacers. Ribs in this direction that are slightly larger than the spacer diameters would reduce the HPD to 0.72", a near 70% reduction in bonding distortion. The full results of the trade study, along with distortion and mass increase efficiencies, is shown in Table 3-2.

Table 3-2 Trade Study Summary of Mirror Stiffening Methods

Bonding Trial	Bonding (arc-sec)		Total Mirror Mass (kg)	Mass Increase (kg)	Distortion Reduction		Efficiency (%HPD reduction/kg added)	Efficiency (%RMS reduction/kg added)
	HPD	RMS			HPD	RMS		
thin (.9/.8)	2.35	7.40	0.0330		N/A			
thick (2/2.4)	0.46	2.72	0.0851	0.0521	80%	63%	15.45	12.15
full isogrid	0.99	3.02	0.0550	0.0220	58%	59%	26.29	26.89
azimuthal ribs	2.09	4.11	0.0445	0.0114	11%	44%	9.66	38.83
azimuthal ribs - edges only (3mm)	2.89	8.30	0.0362	0.0031	-23%	-12%	-73.55	-38.93
azimuthal ribs - posts only (8mm)	3.56	4.58	0.0414	0.0083	-51%	38%	-61.84	45.77
axial ribs	0.50	3.00	0.0466	0.0135	79%	59%	58.15	43.92
axial ribs - edges only (3mm)	1.44	6.98	0.0362	0.0031	39%	6%	123.94	18.17
axial ribs - edges only (8mm)	0.92	6.90	0.0434	0.0104	61%	7%	58.43	6.49
axial ribs - posts only (8mm)	0.72	3.10	0.0434	0.0104	69%	58%	66.60	55.80
Bond pads - 8mm square	2.26	4.42	0.0347	0.0017	4%	40%	22.98	241.67
Bond pads - 6mm circle	2.62	4.62	0.0337	0.0007	-11%	38%	-164.77	538.76

## 4. CONCLUSIONS

The conflicting needs of structural robustness and minimal distortion in the critical bonding locations continue to pose a significant challenge to the technology development of polished silicon X-ray optics. The measured and correlated epoxy shrinkage values and dependence on precision geometry control led to significant distortion when the bonds are made strong enough to survive launch environments. Potential solutions to these conflicting needs have been identified, including stiffening of the mirror substrates. Additional options would include isolating the mirrors from each other, eliminating the stacking method that requires significant strength at the base, which could be achieved with a novel mounting approach, possibly including flexures to further reduce bonding distortion. This would allow smaller bonds, which have been shown structurally sound in vibration tests that do not include the weight of many additionally stacked mirrors.

## REFERENCES

- [1] Zhang, W. W., et al., “Single Crystal Silicon X-ray Optics for Astronomy: high resolution, light weight, and low cost,” SPIE Proc, Vol. 12181-36, these proceedings, (2022).
- [2] Tutt, J. H., et al., “The Off-plane Grating Rocket Experiment (OGRE) system overview,” SPIE Proc, Vol 10699, p. 106996H, (2018).
- [3] Zhang, W. W., et al., “STAR-X: Survey and Time-domain Astrophysical Research eXplorer,” SPIE Proc, Vol. 12181-82, these proceedings, (2022).
- [4] Gaskin, J. A., et al., “The Lynx X-ray Observatory: concept study overview and status,” SPIE Proc, Vol 10699, p. 106990N, (2018).
- [5] Riveros, R.E., et al., “Fabrication of Lightweight Silicon X-ray Mirrors,” SPIE Proc, Vol. 12181-37, these proceedings, (2022).
- [6] Zhang, W. W., et al., “Next Generation X-ray Optics for Astronomy: High Resolution, Light Weight, and Low Cost,” SPIE Proc, Vol. 11119, p. 1111907, (2019).
- [7] Chan, K.W., et al., “Mirror alignment and integration for high-resolution astronomical x-ray telescopes,” SPIE Proc, Vol. 12181-214, these proceedings, (2022).
- [8] Solly, P.M., et al., “Structural Analysis and Testing of Silicon X-ray Mirror Modules,” SPIE Proc, Vol. 11119, p. 111190B, (2019).
- [9] McClelland, R. S., et al, “Design and Analysis of Modules for Segmented X-ray Optics,” SPIE Proc, Vol 8443, p. 84433Y, (2012).
- [10] GSFC-STD-7000A, “General Environmental Verification Standard (GEVS),” (2013).